Environ. Eng. Res. 2021; 26(6): 200524
https://doi.org/10.4491/eer.2020.524

pISSN 1226-1025
eISSN 2005-968X

Research

Photocatalytic degradation of flumequine by N-doped TiO_2 catalysts under simulated sunlight

Xiaolan Zeng[1,2†], Xiaozi Sun[1], Yan Wang[1]

[1]*College of Chemistry and Chemical Engineering, Xinyang Normal University, Xinyang 464000, China*
[2]*Henan Key Laboratory for Synergistic Prevention of Water and Soil Environmental Pollution, Xinyang Normal University, Xinyang 464000, China*

ABSTRACT

Flumequine (FLU) is one of the most used fluoroquinolone antibiotics in intensive aquaculture, however, it has become a typical pollutant in water environment at present due to inappropriate use. Therefore, it is necessary to develop facile techniques for efficient degradation of FLU. In this work, three N-doped TiO_2 photocatalysts were synthesized for degradation of FLU. The obtained photocatalysts were characterized using scanning electron microscopy (SEM), X-ray diffraction (XRD), X-ray photoelectron spectroscopy (XPS), Raman spectrum and UV-Vis diffuse reflection spectra (UV-Vis-DRS). The XRD and XPS results from NH_4NO_3-doped catalyst (TiO_2/AN) confirmed that NO_3^- ions were successfully incorporated into the lattice of TiO_2. The TiO_2/AN sample exhibited higher photocatalytic performance than other N-doped catalysts under simulated sunlight irradiation, and 100% removal efficiency of FLU was achieved after 4 hours of illumination. The photogenerated holes (h^+) and hydroxyl radicals ($^{\bullet}OH$) are main reactive species involved in the photocatalytic degradation of FLU. Eight intermediates for photocatalytic degradation of FLU were detected and their toxicities to aquatic organisms were predicted. This study might have important implications for further research on the removal of fluoroquinolone antibiotics in wastewater.

Keywords: Active species, Degradation mechanism, Flumequine, N-doped TiO_2, Photocatalytic degradation

1. Introduction

Antibiotic drugs have been widely used to treat human and veterinary diseases of bacterial infections since their development for performing a biological effect. However, they have been frequently detected in water environment due to inappropriate use in recent decades [1-5]. Recently, Feng and co-authors have pointed out that many antibiotics are pseudo-persistent pollutants of emerging concern owing to its potential toxicity to non-target species, the development of antibiotic-resistant bacteria and chronic inhibitory effects on growth [6]. Fluoroquinolones (FQs) is one of the most widely employed class of antibiotics with bactericidal action. Particularly, flumequine (FLU) is one of the most used FQs in intensive aquaculture. Since FLU is difficult to be biodegradable naturally [7, 8], it remains active in sediments for extended time periods, producing negative environmental impacts. FLU has been extensively found in surface water and municipal wastewater (2.5–50 ng L^{-1}) and in soil (6.9 mg g^{-1}) [9-13]. Antibiotics such as FLU cannot be often eliminated completely by conventional wastewater treatment systems due to low degradation efficiency [14]. Therefore, it is extremely pressing to develop effective methods to remove FLU from aqueous environment.

Advanced oxidation processes (AOPs) have been successfully applied to remove residual antibiotics in water environment due to their high ability to oxidize pollutants with different structures [1, 3, 15-20]. AOPs mainly include photocatalytic, chemical and electro-chemical methods and combined chemical and biological technology, which can generate a variety of active oxygen species such as hydroxyl radicals ($^{\bullet}OH$), sulfate radicals ($SO_4^{\bullet-}$) and superoxide radicals ($O_2^{\bullet-}$) [21]. Among various AOPs, the photocatalytic method has become an emerging and promising method for the removal of antibiotics in aqueous environment. Titanium dioxide (TiO_2) is one of the most common used photocatalysts owing to its low cost, non-toxicity, mechanical robustness, and environmental friendliness [22, 23]. However, the wide band gap (E_g = 3.2 eV for anatase) and the high recombination rate of photogenerated electron-hole pairs (e^-/h^+) became its two hindrances to high photocatalytic performance [24, 25]. Thus, the structural modification

Received September 20, 2020 **Accepted** November 20, 2020

† Corresponding author
Email: zxl6688@163.com
Tel: +86-0376-6390702

or doping of TiO_2 was considered as a good method to improve its response to the sun light and hence the photocatalytic activity.

Various TiO_2-based photocatalysts by metallic or/and non-metallic ions doping and codoping have been successfully used for the degradation of organic pollutants [26-30]. Among various doping methods, nitrogen doping has been considered as one of the most encouraging due to comparable atomic size to oxygen and small ionization energy of nitrogen atom [31]. Some studies confirmed that nitrogen doping can enhance the visible light absorption of TiO_2 or/and suppresses the recombination rate of e^-/h^+, resulting in an enhancement of photocatalytic performance compared to pure TiO_2 [32-34]. Nieto et al. [35] synthesized N-doped TiO_2 in the presence of urea (U-TiO_2) by using sol-gel technique and they found that the significant effect of U-TiO_2 in the removal of FLU in water system is mainly its adsorption phenomena. Asahi et al. [32] reported that N doping of TiO_2 by annealing the TiO_2 powders in a NH_3/Ar gas mixture leads to an increase of photocatalytic activity of TiO_2 under visible light. Thus, N-doped TiO_2 can be seen as a promising photocatalyst for environmental remediation and other applications. However, there are very few studies on the use of N-doped TiO_2 catalysts for photocatalytic degradation of FLU. On the other hand, the preparation methods of N-doped TiO_2 catalysts and the selection of N sources need to be further expanded. Therefore, it is necessary to develop facile techniques for synthesizing N-doped TiO_2 with different N sources and excellent activity on photocatalytic degradation of FLU.

In the present work, we conducted a comprehensive exploration on the preparation of N-doped TiO_2 catalysts with different N sources using a simple method and their application for the photocatalytic degradation of FLU. The main objectives of this study are as follows: (1) to synthesize a new N-doped TiO_2 catalyst with excellent photocatalytic activity on degradation of FLU and high stability, (2) to investigate the degradation kinetics and the main reactive species in the photodegradation process of FLU involving N-doped TiO_2 catalysts, and (3) to determine the plausible intermediates and degradation pathways in the photodegradation of FLU and predict the toxicities of FLU and these intermediates to some aquatic organisms.

2. Material and Methods

2.1. Materials

FLU (purity > 98%) was provided by J&K Chemical Ltd. Methanol and formic acid (FA) were purchased from Merck (Darmstadt, Germany) and were of HPLC grade. Other chemicals used in this study such as $Ti(SO_4)_2$, HCl, NaOH, *p*-benzoquinone (*p*-BQ), urea ($CO(NH_2)_2$, U), ammonium nitrate (NH_4NO_3, AN), ammonium chloride (NH_4Cl, AC), $AgNO_3$ and *tert*-butyl alcohol (TBA) were analytical reagent grade and used without further purification. A Milli-Q Plus system (Millipore, Bedford USA) was employed to prepare ultrapure water (> 18.2 MΩ cm), which was used throughout all experiments.

2.2. Preparation of Photocatalysts

N-doped TiO_2 catalysts were synthesized by using precipitation combined with thermal decomposition method. The specific steps are as follows: First, using $Ti(SO_4)_2$ (purity ≥ 96%) as a Ti precursor and NaOH (2 M) as precipitator, after the pH of the mixed solution rose to 10 in the precipitation process, then the precipitation cakes were filtrated at vacuum condition, washed using ultrapure water four times and dried at 80℃ overnight. The resultant sample was crushed to obtain fine powder. Second, 1.0 g of the sample powder obtained above and 1.0 g of nitrogenous compounds including $CO(NH_2)_2$, NH_4Cl or NH_4NO_3 were mixed uniformly and then milled thoroughly in an agate mortar, respectively. The resultant mixture was transferred into porcelain crucible for calcination at 450℃ for 2 h at a heating rate of 4 ℃/min in a muffle furnace, and then cooled down to room temperature. The formed product was further crushed. Thus, N-doped TiO_2 catalysts were obtained and signified as TiO_2/U, TiO_2/AC, or TiO_2/AN, respectively. For comparison, the undoped TiO_2 was also synthesized using the same method in the absence of dopants.

2.3. Characterization Methods

Scanning electron microscopic (SEM) instrument (FEI, Netherlands) was used to observe the morphology of the prepared samples. The powder crystalline structures of the samples were obtained using Smart lab 9 X-ray diffractometer (Rigaku, Japan) with Cu Ka (0.15406 nm) X-ray source. Raman spectra of these samples were collected using HORIBA HR800 Raman spectrometer and the intensity data were collected from 100 to 800 cm^{-1}. The chemical states of the samples were investigated by carrying out X-ray photoelectron spectroscopy (XPS) determination employing a PHI 5000 Versa Probe system (ULVAC-PHI, Japan) with Al Kα radiation source. The C 1s level at 284.6 eV was used as an internal standard to correct the shift of binding energy due to relative surface charging. The UV–Vis diffuse reflectance spectra (UV-Vis-DRS) of the samples were obtained via UV-visible spectrophotometer (PerkinElmer, Lambda-950) employing $BaSO_4$ as a reference material.

2.4. Photocatalytic Activity Measurements

All experiments were carried out in a XPA-7 multi-tube agitated photochemical reactor (Xujiang Technology Co., Ltd. Nanjing, China). The photocatalytic activity of the samples was assessed by degrading FLU in aqueous solution under 500 W xenon light irradiation, and its light intensity at the sample position was about 48.0 mW cm^{-2}. The photochemical reactor is equipped with water circulation cooling device to control the reaction temperature at 25 ± 1ºC and further details of XPA-7 can be found in our previous work [36]. In a typical experiment, a 10 mg of sample was added into a quartz photo-reactor containing 50 mL FLU solution (10 mg L^{-1}). Prior to irradiation, the obtained suspension was stirred magnetically for 30 min in the dark to ensure the establishment of adsorption/desorption equilibrium. At prescribed time intervals, 1 mL sample solution was extracted and immediately filtered through a 0.22 μm filter into a brown HPLC vial for further analysis. In the experiment, the initial pH value of the reaction solution was adjusted to pH = 7 ± 0.2 using HCl and NaOH. All experiments were performed in triplicate. To estimate the catalytic stability and reusability of the prepared N-doped TiO_2 catalysts, the recycling

experiments for photocatalytic activity measurements of the catalyst with the highest catalytic performance were conducted. The catalyst was collected by centrifugation after each run and then washed with ultrapure water three times. The catalyst solids were left and the fresh FLU reaction solution was added to the reaction tube, followed by the next run.

2.5. Analytical Methods

An HPLC UV (Agilent Technologies, Series 1200) system equipped with an Agilent ZORBAX SB-C18 column (5 μm, 4.6×150 mm) was used for monitoring FLU concentration. The maximum absorbance wavelength for FLU was 238 nm. The isocratic elution was methanol and 0.3% formic acid in water (v/v = 70:30) at a flow rate of 1 mL min^{-1}. Total organic carbon (TOC) determinations were carried out in a Shimadzu 5000A TOC analyzer.

The degradation products of FLU were analyzed by high resolution liquid chromatography time of flight mass spectrometry (LC-QTOF-MS) using ultra performance liquid chromatography tandem-mass spectrometry (UPLC-MS/MS, Waters Corp., USA). A BEH C18 column (2.1×50 mm, 1.7 μm) was used for chromatographic separation. The mobile phase consisting of 0.1% formic acid in water (A) and acetonitrile (B) was eluted at 0.3 mL min^{-1}. Mass spectrometric analysis was carried out with a G2-XS-QTOF MS operating in a positive ion mode by an electrospray ion source. Mass range of TOF MS was set at *m*/*z* from 100 to 600. The other mass parameters were set as follows: Capillary voltage: 3.0 kV, source temperature: 100℃, desolvation gas flow rate: 800 L h^{-1} and desolvation temperature: 350℃.

2.6. Determination of Active Components ($^{\bullet}OH$, $O_2^{\bullet-}$, e^- and h^+)

In order to evaluate the role of the main reactive species including hydroxyl radical ($^{\bullet}OH$), superoxide radical ($O_2^{\bullet-}$), photogenerated electrons (e^-) and positive hole (h^+) during the photocatalytic reactions, four scavengers including TBA, *p*-BQ, $AgNO_3$ and FA were added to the FLU solutions containing catalyst to capture $^{\bullet}OH$, $O_2^{\bullet-}$, e^-, and h^+, respectively [37-39]. The detailed step was as follows: 10 mg of as-prepared catalyst sample was dispersed in the 50 mL of FLU aqueous solution (10 mg L^{-1}), and then 38.3 mM TBA, 0.38 mM *p*-BQ, 4.0 mM $AgNO_3$ or 1.0 g L^{-1} FA was added into reaction system, respectively. The choice of the concentrations of TBA, *p*-BQ, $AgNO_3$ and FA was referred to a previous report [36]. The analytical method was the same as that used in the evaluation of photocatalyst activity mentioned above.

3. Results and Discussion

3.1. Catalysts Characterization

The surface morphologies of the four as-synthesized samples were examined using SEM technique and the results are shown in Fig. 1. The surface topography of these samples varied widely. The surface of pure TiO_2 particles appeared rough and not uniform (Fig. 1(a)). Compared to pure TiO_2, the TiO_2/U sample particles were tightly packed and layered, resulting in bad adsorption capacity (Fig. 1(b)). For TiO_2/AC sample, although its particle size was obviously smaller than those of pure TiO_2 and TiO_2/U, there was

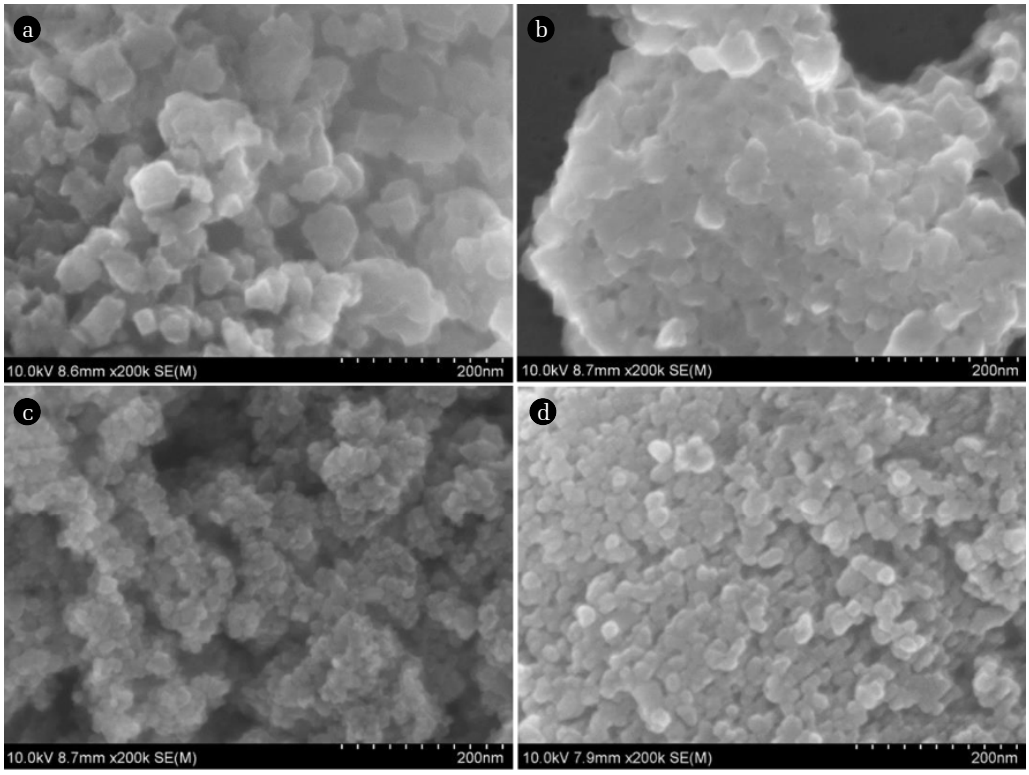

Fig. 1. SEM images of the as-synthesized (a) pure TiO_2, (b) TiO_2/U, (c) TiO_2/AC and (d) TiO_2/AN.

agglomeration in it (Fig. 1(c)). Compared to the three samples mentioned above, the particles of TiO_2/AN sample (Fig. 1(d)) exhibited spherical, highly dispersed and evener particle size distribution in the range of 9–13 nm. Thus, it was expected to have high photocatalytic activity.

XRD measurements were performed to identify the crystal structures of the four samples (pure TiO_2, TiO_2/U, TiO_2/AC and TiO_2/AN) and the results are shown in Fig. 2(a). The XRD spectra results of these samples indicated that the main diffraction peaks at 25.3°, 37.9°, 48.1°, 54.0°, 55.1° and 62.9° are attributed to (101), (004), (200), (105), (211) and (204) lattice planes of anatase of TiO_2, agreeing well with the standard JCPDS No. 21-1272, respectively. Specifically, all diffraction peaks of pure TiO_2 and TiO_2/U samples belong to the crystalline phase of anatase of TiO_2. However, for TiO_2/AC and TiO_2/AN samples, some new diffraction peaks were observed in their XRD patterns. The new diffraction peaks at about 27.4°, 31.7°, 45.4°, 56.5° and 66.2° were observed along with the anatase phase peaks for TiO_2/AC sample, which is attributed to the (111), (200), (220), (222) and (400) planes of NaCl (JCPDS No. 75-0306), respectively. At the same time, for TiO_2/AN sample, new diffraction peaks at about 29.4°, 31.8°, 35.4° and 42.5° were observed along with the anatase phase peaks and they may belong to the planes (104), (006), (110) and (202) of $NaNO_3$ (JCPDS No. 72-1213), respectively. It is worth noting that $NaNO_3$ and NaCl were generated by the reactions between Na^+ and the anions in the dopants NH_4NO_3 and NH_4Cl, respectively, where Na^+ comes from the precursor NaOH used in the preparation of TiO_2. In addition, two diffraction peaks of NH_4NO_3 (JCPDS No. 74-0972) were observed at 22.8 ° and 27.8° for (111) and (210) planes, respectively. These give the evidence that NH_4NO_3 was doped successfully into the crystal structure of TiO_2, including N^{5+} (NO_3^-) and N^{3-} (NH_4^+), which is consistent with the conclusion of XPS analysis discussed later. It may be one of the reasons for the improvement of the photocatalytic activity of TiO_2/AN sample because NO_3^- and NH_4^+ can trap photogenic electrons (e^-) or photogenic holes (h^+) to prevent e^-/h^+ pairs recombination and this helps to promote the charge separation. Based on the Scherrer's formula and XRD peak at about 25.3° of (101) plane, the average crystallite sizes of TiO_2, TiO_2/U, TiO_2/AC and TiO_2/AN samples were calculated, and they were 19.9, 16.1, 14.2 and 11.0 nm, respectively. These results showed that the average particle size of TiO_2/AN sample is less than that of other three samples. Thus, it illustrates that NH_4NO_3 doping can inhibit better the crystal growth of anatase TiO_2, which helps to improve the photocatalytic activity of TiO_2.

Fig. 2(b) displays the Raman spectra of TiO_2, TiO_2/U, TiO_2/AC and TiO_2/AN samples. Raman peak shifts at about 145, 397, 516, 639 cm^{-1} stem from the characteristic Raman peaks of anatase phase [36, 40, 41], demonstrating that the main phase structure of the prepared samples was anatase. No peak attributed to nitrogen-containing phases was detected in the doped TiO_2 catalysts, indicating that nitrogen was highly dispersed on the TiO_2 surface. It can be observed that the peak at about 145 cm^{-1} for the doped TiO_2 samples became wider in the following order TiO_2 < TiO_2/U < TiO_2/AC < TiO_2/AN, suggesting that their particles size decreases correspondingly and the results of Raman analysis are in good agreement with the XRD results (see Fig. 2(a)).

The surface composition and chemical states of elements in the NH_4NO_3-doped TiO_2 sample were further characterized by XPS and shown in Fig. 3. Fig. 3(a) presented the XPS full spectrum survey of the sample and shows that the species like C, N, O, Ti and Na are predominantly present in the wide XPS spectrum. Taking the C 1s peak (286.4 eV) as a benchmark, the obtained binding energies were corrected. The C 1s peak may come from exterior hydrocarbon from XPS instrument itself [1]. Based on the XPS data, the atomic concentrations of Ti, O, Na and N for the TiO_2/AN sample were estimated to be about 9.8, 47.8, 12.5 and 9.2 atom%, respectively. Na 1s peak at about 1,071.3 eV comes from the precipitant NaOH used during the synthesis of TiO_2 [42]. As shown in Fig. 3(b), two peaks located at 458.1 and 463.9 eV in Ti 2p XPS spectrum belong to Ti $2p_{3/2}$ and Ti $2p_{1/2}$, respectively. The two peaks have slightly lower binding values than those of classical spectrum of Ti^{4+} in TiO_2 [43], suggesting NO_3^- doping has negligible effect on the chemical valence status of Ti. Fig. 3(c) indicates that two N 1s peaks are observed at 407.32 eV and 403.35 eV, implying that there are two kinds of doped N species. The peaks at 407.32 eV is assigned to the binding energy of N^{5+} in NO_3^- ions, which confirms that NO_3^- can be incorporated into the TiO_2 lattice, the other at 403.35 eV is attribute to N^{3-} in NH_4^+. The relative magnitude of their peak areas suggested that N^{5+} is main N doping species. As shown in Fig. 3(d), the XPS spectra

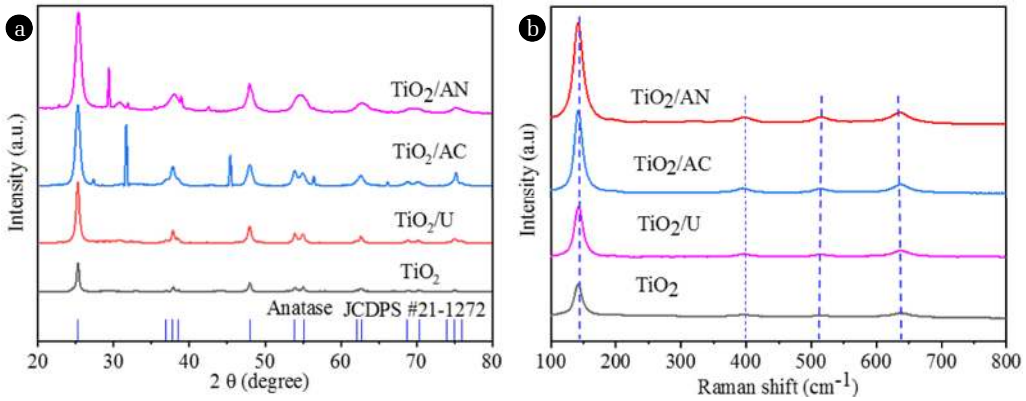

Fig. 2. XRD patterns (a) and Raman spectrums (b) of the as-synthesized pure TiO_2, TiO_2/U, TiO_2/AC and TiO_2/AN samples.

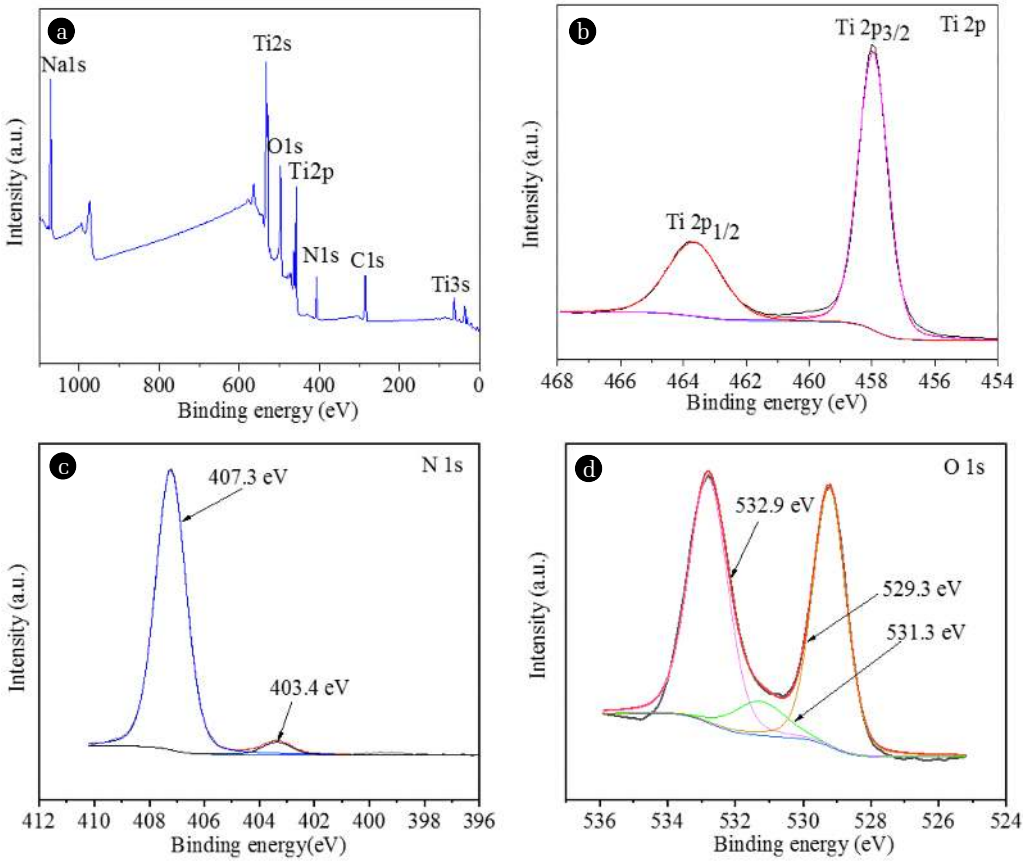

Fig. 3. The XPS spectra of TiO_2/AN sample. (a) The survey spectra, (b), (c) and (d) are high resolution spectra for Ti2p, N1s and O1s, respectively.

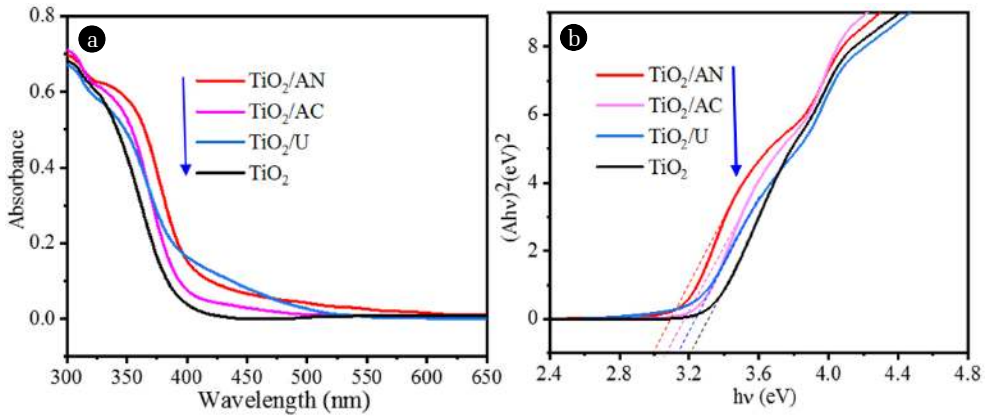

Fig. 4. UV-Vis diffuses reflectance spectra (a) and the Tauc plot (b) of as-synthesized catalysts.

of O 1s can be fitted into three different peaks at binding energy values of 532.9, 531.3 and 529.3 eV corresponding to surface chemisorbed oxygen, oxygen vacancies and lattice oxygen respectively. The peak at 532.9 eV belongs to O atoms of NO_3^- ions, demonstrating successful preparation of NO_3^--doped TiO_2.

UV–Vis diffuse reflectance spectra (UV-Vis-DRS) of as-synthesized samples are indicated in Fig. 4. A weak absorption band between 400 and 520 nm was found for TiO_2/U, TiO_2/AC and TiO_2/AN, suggesting that the light absorption performance of TiO_2/U, TiO_2/AC and TiO_2/AN is better than that of TiO_2. On the other hand, the forbidden band width values (E_g) for TiO_2, TiO_2/U, TiO_2/AC and TiO_2/AN can be estimated using a Tauc plot based on the UV-Vis-DRS data, and the corresponding values are 3.22, 3.15, 3.10 and 3.01 eV, respectively. Therefore, N-doping can narrow the band gap of TiO_2 and enhance its performance for photocatalytic degradation of FLU, especially for TiO_2/AN. The same result was also found for urea or thiourea-doped TiO_2 prepared using the sol–gel technique, and the shift of the light absorption profile in

N-doped TiO_2 may be associated to the presence of manifold surface states close to the valence band edge [35].

3.2. Photocatalytic Activity

3.2.1. Comparison of photocatalytic activity of N-doped TiO_2 with different nitrogen sources

The efficiencies for FLU degradation using TiO_2, TiO_2/U, TiO_2/AC or TiO_2/AN as photocatalyst are displayed in Fig. 5(a). When pure TiO_2 was used as catalyst, the removal efficiency of FLU is only about 12% after 4 hours of illumination, while the corresponding values for TiO_2/U, TiO_2/AC and TiO_2/AN are about 25%, 98% and 100%, respectively. This result indicated that all of three N-doped TiO_2 samples show higher photocatalytic performance than pure TiO_2 for FLU removal, and the order of FLU removal efficiency for different photocatalysts is as follows: TiO_2/AN > TiO_2/AC > TiO_2/U > TiO_2. Meantime, it can be seen from Fig. 5(b) that the calculated apparent first-order rate constants (k_{app}) in the presence of TiO_2/AN catalyst is about 35, 16 or 1.4 times higher than that of pure TiO_2, TiO_2/U or TiO_2/AC, respectively, where the k_{app} values could be obtained from the slope of regression line by plotting $-\ln(C_t/C_0)$ vs. irradiation time (t). These results suggested that TiO_2/AN sample exhibits the highest photocatalytic activity in the removal process of FLU. This may be because that two different valence states of nitrogen (N^{5+} and N^{3-}) exist in this catalyst and prefer to capture photogenerated electrons, resulting in a reduce of recombination rate of the photogenerated electron and hole pairs

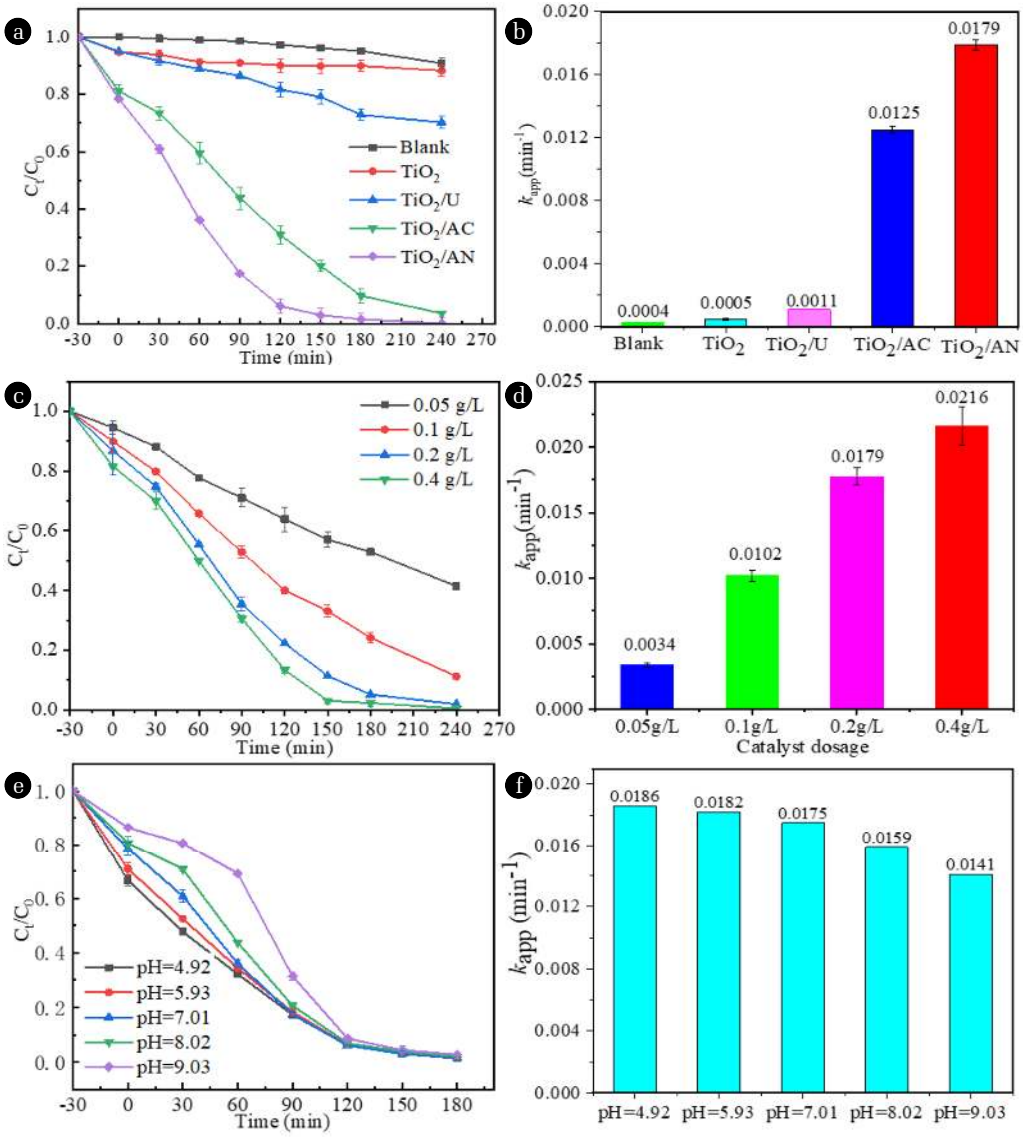

Fig. 5. (a)-(b) Comparison of photocatalytic degradation of FLU under simulated sunlight with 0.2 g L^{-1} of the different catalysts, (c)-(d) effect of TiO_2/AN dosage on the photocatalytic degradation of FLU, (e)-(f) effect of the initial solution pH on the photocatalytic degradation of FLU using TiO_2/AN as photocatalyst. Experimental conditions: $[FLU]_0$ = 10 mg L^{-1} and $[pH]_0$ = 7.0 ± 0.1.

and hence an improvement of the degradation efficiency of FLU. It should be noted that the first 30 minutes in the degradation efficiency curves of Fig. 5(a) (Abscissa from -30 to 0 min) is actually a dark adsorption process without light illumination. It can be seen from Fig. 5(a) that the adsorption rates of FLU by TiO_2 and TiO_2/U were less than 5% after adsorption equilibrium, while that for TiO_2/AC or TiO_2/AN was about 18% or 23%, respectively. This result indicated that the stronger the catalyst adsorbs FLU in the solution, the higher its photocatalytic degradation ability to FLU. However, in general, the adsorption ability of several catalysts involved in this work on FLU in solution was not strong, which suggests that the main effects of TiO_2/AN and TiO_2/AC on the removal of FLU are their photocatalytic performance, and the adsorption effect is relatively smaller. In addition, a direct photolysis experiment without adding any catalyst was also performed, and the result indicated that the degradation efficiency of FLU was less 7% after 4 hours of illumination (marked as "Blank" in Fig. 5(a)). Thus, the contribution of direct photolysis to degradation of FLU is negligible.

3.2.2. Effect of TiO_2/AN dosage on photocatalytic degradation of FLU

Fig. 5(c) and (d) show the effect of TiO_2/AN catalyst dosage (dosage c = 0.05, 0.1, 0.2 and 0.4 g L^{-1}) on the FLU degradation process. Fig. 5(c) indicates that the FLU removal efficiency increases with increasing the dosage of catalyst. Obviously, this enhancement in removal efficiency was due to an increase of the number of active sites on the used photocatalysts. In addition, their k_{app} values for initial dosages of TiO_2/AN (0.05, 0.1, 0.2 and 0.4 g L^{-1}) were observed as 0.0034, 0.0102, 0.0179, and 0.0216 min^{-1}, respectively (Fig. 5(d)). It can also be found that the k_{app} is nearly proportional to the dosage of catalyst and the fitting equation can be expressed as k_{app} = 0.0062c - 0.0023 (R^2 = 0.982). Considering that when the catalyst dosage was 0.2 g L^{-1}, a near complete removal of FLU was achieved after 4 hours of irradiation, the TiO_2/AN dosage was kept at 0.2 g L^{-1} for FLU degradation in subsequent experiments.

3.2.3. Effect of initial pH on photocatalytic degradation of FLU

Fig. 5(e) and (f) show the effect of pH (pH = 4.92, 5.93, 7.01, 8.02 and 9.03) on the FLU degradation. Fig. 5(e) indicates that the removal efficiency of FLU at the initial stage of degradation decreases with increasing the solution pH from 4.92 to 9.03. However, when the degradation time reaches 3 hours, regardless of the initial pH value, the degradation rate of FLU exceeds 90% in all five experiments. Moreover, the k_{app} values for the different initial pH were obtained as 0.0186, 0.0182, 0.0175, 0.0159 and 0.0141 min^{-1}, respectively (see Fig. 5(f)). Based on the above results, it can be inferred that the initial pH has only little effect on photocatalytic degradation of FLU when TiO_2/AN was employed as a photocatalyst.

3.2.4. Mineralization analysis

TOC determinations were carried out to evaluate the mineralization of FLU degradation when TiO_2/AN was used as a photocatalyst. The results are displayed in Fig. S1. The TOC removal rate was found to be 81.2% after 4 h of irradiation. However, the TOC removal is relatively lower compared to the removal efficiency of FLU, suggesting that some intermediates were generated during FLU degradation, which will be discussed later.

3.3. Photocatalyst Stability

Four recycling experiments for degradation of FLU were performed to assess the photocatalytic stability and reusability of the TiO_2/AN catalyst. The specific method of reusing TiO_2/AN catalyst is as follows: 50 mL of FLU solution (10 mg L^{-1}) and 10 mg fresh catalyst was added to the reaction vessel, and the suspension was left to equilibrium adsorption for 30 min in the dark and then subject to 500 W Xe light irradiation for 4 hours. FLU degradation was monitored at prescribed time intervals and the first cycle was completed. The catalyst was collected by centrifugation and then washed with ultrapure water three times. After washing, the water was removed as much as possible, only the catalyst solids were left and the fresh FLU reaction solution of 50 mL was added to the reaction tube, followed by the second run and this procedure was repeated for three cycles. The results are depicted in Fig. 6. FLU was almost completely removed by using TiO_2/AN as catalyst after 4 hours irradiation at the first cycle, and FLU conversion efficiency remained at 91.8% with TiO_2/AN catalyst after four cycles. The reduction in catalytic performance of TiO_2/AN catalyst may originate from the catalyst loss due to washing process. Thus, the photocatalytic degradation of FLU by TiO_2/AN was affected slightly during four consecutive runs under 500 W Xe light irradiation, indicating good photocatalytic stability of the TiO_2/AN catalyst.

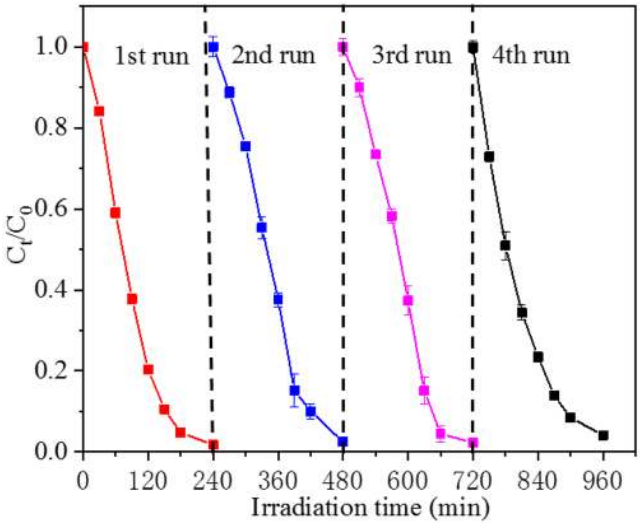

Fig. 6. The cycling stability of TiO_2/AN photocatalyst for FLU degradation.

3.4. Role of Reactive Species in the Photocatalytic Degradation of FLU

The reactive species quenching tests were performed to distinguish the major reactive components including $^{\bullet}OH$, $O_2^{\bullet-}$, photogenerated holes (h^+) and photogenerated electron (e^-) during the photocatalytic degradation process of FLU with TiO_2/AN as catalyst. In the experiments, TBA, *p*-BQ, FA and $AgNO_3$ were used as scavenges to quench the related active species [37-39] and were separately introduced into the photocatalytic system (TBA for only free $^{\bullet}OH$, *p*-BQ for $O_2^{\bullet-}$, FA for both h^+ and total $^{\bullet}OH$, $AgNO_3$ for e^-, respectively). As shown in Fig. 7(a), the removal of FLU was all inhibited by the addition of these scavengers separately in the FLU solution.

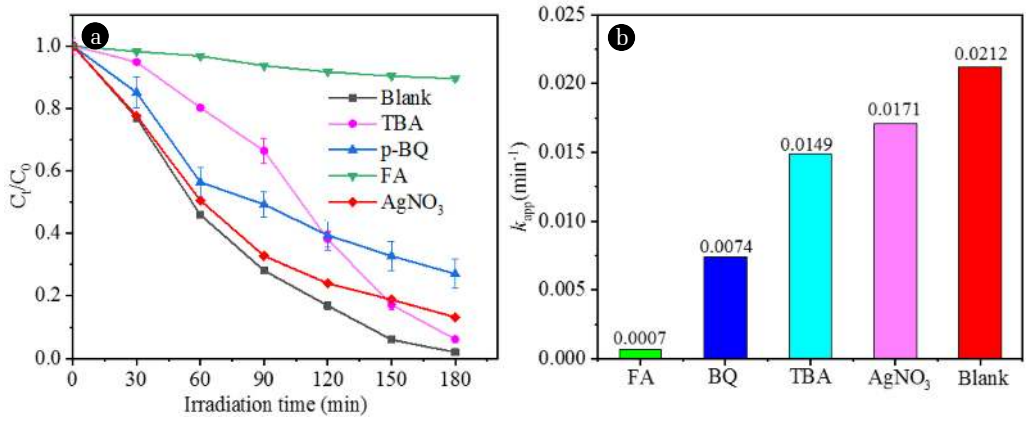

Fig. 7. Reactive species trapping experiments over the prepared TiO_2/AN catalyst. Experimental conditions: $[FLU]_0$ = 10 mg L^{-1}, [catalyst] = 0.2 g L^{-1} and pH~7.0, [TBA] = 38.3 mM, [*p*-BQ] = 0.38 mM, [FA]= 1.0 g L^{-1} and [$AgNO_3$] = 4 mM.

Compared with the blank test, the addition of $AgNO_3$ in the FLU solution has slight inhibitory effect on the removal of FLU. However, the removal of FLU was obviously inhibited by the addition of FA and stronger inhibitory effect were also both observed after the addition of TBA and *p*-BQ. Their k_{app} values for photocatalytic degradation of FLU with or without scavenger were also calculated and displayed in Fig. 7(b). As observed in Fig. 7(b), the efficiency for photocatalytic degradation of FLU was inhibited in the order of FA > *p*-BQ > TBA > $AgNO_3$. These experimental results indicated that both h^+ and $^{\bullet}OH$ are major reactive species in this photocatalytic degradation system and $O_2^{\bullet-}$ also play an important role, while e^- play negligible roles.

3.5. Identification of Degradation Intermediates and Reaction Pathways

The primary intermediates for photocatalytic degradation of FLU were determined by employing the MS^2 scan technique included in LC-TOF-MS. Based on MS data analysis, eight plausible degradation intermediates were detected in the positive mode. Fig. S2 indicates the proposed molecular structures of these intermediates and their fragmentation patterns. Table S1 summarizes their MS data and corresponding retention time. It can be found that small errors exist between the calculated and experimental *m/z* for these suggested molecular formulas. Therefore, the structural assignment for these intermediates is highly reliable, which makes it possible to propose the pathways for photocatalytic degradation of FLU.

Three plausible pathways for photocatalytic degradation of FLU employing TiO_2/AN as photocatalyst were proposed based on the geometric structures of the identified degradation intermediates and displayed in Fig. 8. In the first pathway (pathway I), a propane molecule was removed from the upper saturated heterocyclic ring, resulting in formation of the degradation intermediate P1, which occurs most probably due to attack of h^+ on the saturated ring of FLU. The intermediate P1 was also detected in the previous report on direct photolysis of FLU in water [44]. The next pathway (pathway II) was initiated by the attack of $^{\bullet}OH$ at C7 position of the saturated ring, leading to the formation of hydroxylated intermediate P2. The subsequent hydrogen abstraction of P2 produces another intermediate P3. The intermediates P2 and P3 were also found in the recent study on oxidative degradation of FLU using K_2FeO_4 as oxidant [45]. The third pathway (pathway III) was also triggered by $^{\bullet}OH$ attack, but the attack position is most likely to be on the C3 atom of FLU according to the theoretically calculated electron densities of FLU and our previous research [36, 45], and the resultant intermediate P4 is the isomer of P1. Subsequent substitution of fluorine atom by $^{\bullet}OH$ may occur for P4, resulting in the formation of dihydroxylated intermediate P5. In addition, P4 can also undergo further decarboxylation, demethylation, the opening of the quinolone ring or their combination to yield the intermediates P6, P7 or P8, respectively. The intermediates P4, P6, P7 and P8 were also identified in a recent report [45]. It should be noted that the above decarboxylation processes are likely to occur by a photo-Kolbe pathway with the direct participation of h^+ as shown by the reaction ($RCOO^- + h^+ \rightarrow RCOO^{\bullet} \rightarrow R^{\bullet} + CO_2$), while the opening of the quinolone ring may be initiated by the attack of superoxide radical ($O_2^{\bullet-}$) on the C2-C3 double bond of the quinolone ring.

3.6. Toxicity Evaluation

The ECOSAR program [46] was used to predict acute and chronic toxicities of FLU and proposed degradation intermediates (P1~P8) to fish, daphnids and green algae, and the results are summarized in Table S2. It should be noted that the predicted toxicity data of P1 were marked with "*" in the output result, suggesting that it might be too insoluble to predict the toxicity effect. Therefore, the predicted toxicity data of P1 are not listed in Table S2. It can be seen from Table S2 that FLU has chronic toxicity to three test organisms (1 mg L^{-1} < ChV ≤ 10 mg L^{-1}) according to the Globally Harmonized System of Classification and Labelling of Chemicals, while the degradation intermediates of FLU don't show toxicity in general. Thus, NH_4NO_3-doped TiO_2 could be employed as an adequate catalyst for the photocatalytic degradation of FLU in water and wastewater.

3.7. Comparison with Previous Studies

The photocatalytic degradation of FLU in the aqueous phase have been investigated employing commercialized or modified TiO_2 photocatalysts [8, 35, 47-49]. A comparison for photodegradation of

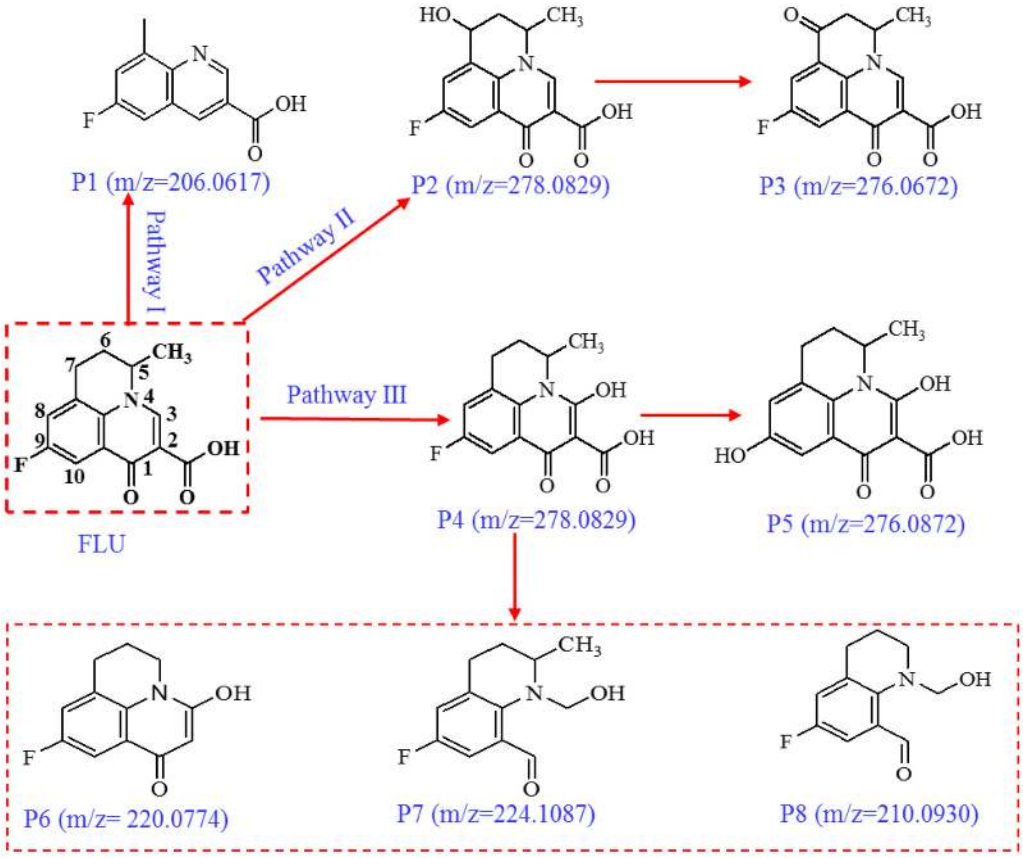

Fig. 8. Proposed photocatalytic degradation pathways of FLU in the presence of TiO_2/AN under simulated sunlight irradiation. Experimental conditions: $[FLU]_0$ = 10 mg L^{-1}, catalyst dosage = 0.2 g L^{-1}, initial pH = 7.0 ± 0.1.

FLU between the present study and these reports was made and is displayed in Table S3. The degradation efficiencies of FLU in these researches using pure anatase TiO_2, thiourea-TiO_2, urea-TiO_2, graphene-TiO_2 or TiO_2/ZnO/Sepiolite catalysts were found to be in the range of 55~100% in 60~240 min of solar-simulated irradiation or UV irradiation, and the TOC removal efficiencies ranged over 35.8~74%. While in the present study, the efficiencies for FLU or TOC removal reached 100% or 81.2 % respectively after 4 h of irradiation. In general, the results of this study are comparable to literature studies.

4. Conclusions

In this study, three N-doped TiO_2 photocatalysts were synthesized by a simple two-step method using $Ti(SO_4)_2$ as Ti source and $CO(NH_2)_2$, NH_4Cl or NH_4NO_3 as N source, respectively. The XRD and XPS observation confirmed the incorporation of NO_3^- ions into the lattice of TiO_2 in TiO_2/AN sample. The TiO_2/AN catalyst exhibited the highest photocatalytic performance in the photocatalytic degradation of FLU under simulated sunlight irradiation and the mineralization rate of FLU reached 81.2 % after 4 h of irradiation. The quenching experiments showed that the active species playing an important role in the photocatalytic degradation of FLU are h^+ and $^{\bullet}OH$. Hydroxylation, decarboxylation, demethylation, ring opening and fluorine substitution were several main degradation patterns for FLU in water. The intermediates for photocatalytic degradation of FLU involving TiO_2/AN catalyst show relatively lower toxicities to fish, daphnids and green algae than FLU generally. Further research on the photocatalytic degradation of other fluoroquinolone antibiotics using TiO_2/AN catalyst is currently underway. Moreover, the use of more other nitrogen sources to prepare N-doped TiO_2 catalysts with high activity and stability is also under consideration.

Acknowledgement

This research was funded by the National Natural Science Foundation of China (Grant No. 21876143), Key Scientific Research Projects of Universities in Henan Province (Grant No. 19B610003) and Nanhu Scholars Program for Young Scholars of XYNU.

Author Contributions

X.Z. (Associate Professor) conceived and designed the study, supervised the experiments execution, reviewed and edited the manu-

script, and undertook all the revision work of the paper. X.S. (Sc.M. student) conceived and designed the study, performed the experiments, and wrote the paper. Y.W. (Professor) reviewed and edited the manuscript. All authors read and approved the manuscript.

References

1. Gul I, Sayed M, Shah NS, et al. Solar light responsive bismuth doped titania with Ti^{3+} for efficient photocatalytic degradation of flumequine: Synergistic role of peroxymonosulfate. *Chem. Eng. J.* 2020;384:123255.
2. Shah NS, Khan JA, Sayed M, et al. Hydroxyl and sulfate radical mediated degradation of ciprofloxacin using nano zerovalent manganese catalyzed $S_2O_8^{2-}$. *Chem. Eng. J.* 2019;356:199-209.
3. Feng M, Yan L, Zhang X, et al. Fast removal of the antibiotic flumequine from aqueous solution by ozonation: Influencing factors, reaction pathways, and toxicity evaluation. *Sci. Total Environ.* 2016;541:167-175.
4. Che H, Che G, Jiang E, Liu C, Dong H, Li C. A novel Z-Scheme CdS/Bi_3O_4Cl heterostructure for photocatalytic degradation of antibiotics: Mineralization activity, degradation pathways and mechanism insight. *J. Taiwan Inst. Chem. Eng.* 2018;91:224-234.
5. Gao P, Munir M, Xagoraraki I. Correlation of tetracycline and sulfonamide antibiotics with corresponding resistance genes and resistant bacteria in a conventional municipal wastewater treatment plant. *Sci. Total Environ.* 2012;421-422:173-183.
6. Feng M, Wang Z, Dionysiou DD, Sharma VK. Metal-mediated oxidation of fluoroquinolone antibiotics in water: a review on kinetics, transformation products, and toxicity assessment. *J. Hazard. Mater.* 2018;344:1136-1154.
7. Speltini A, Sturini M, Maraschi F, Viti S, Sbarbada D, Profumo A. Fluoroquinolone residues in compost by green enhanced microwave-assisted extraction followed by ultra performance liquid chromatography tandem mass spectrometry. *J. Chromatogr. A* 2015;1410:44-50.
8. Palominos R, Freer J, Mondaca MA, Mansill HD. Evidence for hole participation during the photocatalytic oxidation of the antibiotic flumequine. *J. Photoche. Photobio. A: Chem.* 2008;193: 139-145.
9. Reyes-Garcia EA, Sun Y, Raftery D. Solid-state characterization of the nuclear and electronic environments in a boron-fluoride co-doped TiO_2 visible-light photocatalyst. *J. Phys. Chem. C* 2007;111:17146-17154.
10. Tamtam F, Mercier F, Le Bot B, et al. Occurrence and fate of antibiotics in the Seine River in various hydrological conditions. *Sci. Total Environ.* 2008;393:84-95.
11. Ye Z, Weinberg HS, Meyer MT. Trace analysis of trimethoprim and sulfonamide, macrolide, quinolone, and tetracycline antibiotics in chlorinated drinking water using liquid chromatography electrospray tandem mass spectrometry. *Anal. Chem.* 2007;79:1135-1144.
12. Pozo OJ, Guerrero C, Sancho JV, et al. Efficient approach for the reliable quantification and confirmation of antibiotics in water using on-line solid-phase extraction liquid chromatography/tandem mass spectrometry. *J. Chromatogr. A* 2006;1103: 83-93.
13. Tamtam F, van Oort F, Le Bot B, et al. Assessing the fate of antibiotic contaminants in metal contaminated soils four years after cessation of long-term waste water irrigation. *Sci. Total Environ.* 2011;409:540-547.
14. Rodrigues-Silva C, Maniero MG, Rath S, Guimarães JR. Degradation of flumequine by photocatalysis and evaluation of antimicrobial activity. *Chem. Eng. J.* 2013;224:46-52.
15. Zheng X, Xu S, Wang Y, Sun X, Gao Y, Gao B. Enhanced degradation of ciprofloxacin by graphitized mesoporous carbon (GMC)-TiO_2 nanocomposite: Strong synergy of adsorption-photocatalysis and antibiotics degradation mechanism. *J. Colloid. Interf. Sci.* 2018;527:202-213.
16. Feng M, Qu R, Zhang X, et al. Degradation of flumequine in aqueous solution by persulfate activated with common methods and polyhydroquinone-coated magnetite/multi-walled carbon nanotubes catalysts. *Water Res.* 2015;85:1-10.
17. Ge L, Na G, Zhang S, et al. New insights into the aquatic photochemistry of fluoroquinolone antibiotics: Direct photodegradation, hydroxyl-radical oxidation, and antibacterial activity changes. *Sci. Total Environ.* 2015;527-528:12-17.
18. Yan W, Yan L, Jing C. Impact of doped metals on urea-derived g-C_3N_4 for photocatalytic degradation of antibiotics: Structure, photoactivity and degradation mechanisms. *Appl. Catal. B: Environ.* 2019;244:475-485.
19. Kamagate M, Assadi AA, Kone T, Coulibaly L, Hanna K. Activation of persulfate by irradiated laterite for removal of fluoroquinolones in multi-component systems. *J. Hazard. Mater.* 2018;346:159-166.
20. Wang Y, Tian D, Chu W, Li M, Lu X. Nano scaled magnetic $CuFe_2O_4$ as an activator of peroxymonosulfate for the degradation of antibiotics norfloxacin. *Sep. Purif. Technol.* 2019;212: 536-544.
21. Garcia-Segura S, Garrido JA, Rodríguez RM, et al. Mineralization of flumequine in acidic medium by electro-Fenton and photo-electro-Fenton processes. *Water Res.* 2012;46:2067-2076.
22. Cao W, Gui Z, Chen L, Zhu X, Qi Z. Facile synthesis of sulfate-doped Ag_3PO_4 with enhanced visible light photocatalytic activity. *Appl. Catal. B: Environ.* 2017;200:681-689.
23. Lee CG, Javed H, Zhang D, et al. Porous electrospun fibers embedding TiO_2 for adsorption and photocatalytic degradation of water pollutants. *Environ. Sci. Technol.* 2018;52:4285-4293.
24. Cavalcante RP, Dantas RF, Bayarri B, et al. Synthesis and characterization of B-doped TiO_2 and their performance for the degradation of metoprolol. *Catal. Today* 2015;252:27-34.
25. Nie Y, Yu F, Wang L, et al. Photocatalytic degradation of organic pollutants coupled with simultaneous photocatalytic H_2 evolution over graphene quantum dots/Mn-N-TiO_2/g-C_3N_4 composite catalysts: Performance and mechanism. *Appl. Catal. B: Environ.* 2018;227:312-321.
26. Gao XH, Zhou BH, Yuan RF. Doping a metal (Ag, Al, Mn, Ni and Zn) on TiO_2 nanotubes and its effect on Rhodamine B photocatalytic oxidation. *Environ. Eng. Res.* 2015;20:329-335.
27. Yuan RF, Liu D, Wang SN, Zhou BH, Ma FS. Enhanced photocatalytic oxidation of humic acids using Fe^{3+}-Zn^{2+} co-doped TiO_2: The effects of ions in aqueous solutions. *Environ. Eng. Res.* 2018;23:181-188.
28. Putri RA, Safni S, Jamarun N, Septiani U, Kim MK, Zoh KD.

Degradation and mineralization of violet-3B dye using C-N-co-doped TiO_2 photocatalyst. *Environ. Eng. Res*. 2020;25:529-535.
29. Li D, Jia J, Zheng T, Cheng X, Yu X. Construction and characterization of visible light active Pdnano-crystallite decorated and C-N-S-co-doped TiO_2 nanosheet array photoelectrode for enhanced photocatalytic degradation of acetylsalicylic acid. *Appl. Catal. B: Environ*. 2016;188:259-271.
30. Bakar SA; Ribeiro C. A comparative run for visible-light-driven photocatalytic activity of anionic and cationic S-doped TiO_2 photocatalysts: A case study of possible sulfur doping through chemical protocol. *J. Mol. Catal. A: Chem*. 2016;421:1-15.
31. Ansari SA, Khan MM, Ansari MO, Cho MH. Nitrogen-doped titanium dioxide (N-doped TiO_2) for visible light photocatalysis. *New J. Chem*. 2016;40:3000-3009.
32. Asahi R, Morikawa T, Ohwaki T. Visible-light photocatalysis in nitrogen-doped titanium oxides. *Science* 2001;293:269-271.
33. Shie JL, Lee CH, Chiou CS, Chen YH, Chang CY. Photocatalytic characteristic and photodegradation kinetics of toluene using N-doped TiO_2 modified by radio frequency plasma. *Environ. Technol*. 2014;35:653-660.
34. Vaiano V, Sacco O, Sannino D, Ciambelli P. Nanostructured N-doped TiO_2 coated on glass spheres for the photocatalytic removal of organic dyes under UV or visible light irradiation. *Appl. Catal. B: Environ*. 2015;170-171:153-161.
35. Nieto J, Freer J, Contreras D, Candal RJ, Sileo EE, Mansilla HD. Photocatalyzed degradation of flumequine by doped TiO_2 and simulated solar light. *J. Hazard. Mater*. 2008;155:45-50.
36. Zeng X, Sun X, Yu Y, Wang H, Wang Y. Photocatalytic degradation of flumequine with B/N codoped TiO_2 catalyst: Kinetics, main active species, intermediates and pathways. *Chem. Eng. J*. 2019;378:122226.
37. Cavalcante RP, Dantas RF, Bayarri B, et al. Photocatalytic mechanism of metoprolol oxidation by photocatalysts TiO_2 and TiO_2 doped with 5% B: Primary active species and intermediates. *Appl. Catal. B: Environ*. 2016;194:111-122.
38. Qi XM, Gu ML, Zhu XY, et al. Fabrication of $BiOIO_3$ nanosheets with remarkable photocatalytic oxidation removal for gaseous elemental mercury. *Chem. Eng. J*. 2016;285:11-19.
39. Chen Y, Peng RF, Shen TD, Tong SP, Ma CA. A promising ozone-based advanced oxidation process for effective generation of hydroxyl radicals in acidic solution. *Sep. Purif. Technol*. 2015;151:269-275.
40. Tian GH, Fu HG, Jing LQ, Xin BF, Pan K. Preparation and characterization of stable biphase TiO_2 photocatalyst with high crystallinity, large surface area, and enhanced photoactivity. *J. Phys. Chem. C* 2008;112:3083-3089.
41. Zhang G, Zhang CZ, Nadagouda M, et al. Visible light-sensitized S, N and C co-doped polymorphic TiO_2 for photocatalytic destruction of microcystin-LR, *Appl. Catal. B: Environ*. 2014;144:614-621.
42. Singh I, Birajdar B. Synthesis, characterization and photocatalytic activity of mesoporous Na-doped TiO_2 nano-powder prepared via a solvent-controlled nonaqueous sol–gel route. *RSC Adv*. 2017;7:54053-54062.
43. Zhao B, Wang X, Zhang Y, Gao J, Chen Z, Lu Z. Synergism of oxygen vacancies, Ti^{3+} and N dopants on the visible-light photocatalytic activity of N-doped TiO_2. *J. Photochem. Photobiol. A: Chem*. 2019;382:111928.
44. Sirtori C, Zapata A, Gernjak W, Malato S, Agera A. Photolysis of flumequine: identification of the major phototransformation products and toxicity measures. *Chemosphere* 2012;88:627-634.
45. Feng M, Wang X, Chen J, et al. Degradation of fluoroquinolone antibiotics by ferrate(VI): Effects of water constituents and oxidized products. *Water Res*. 2016;103:48-57.
46. ECOSAR, Program Risk Assessment Division (7403), U.S. Environmental Protection Agency. http://www.epa.gov/oppt/newchems/tools/21ecosar.htm.
47. Paul T, Miller PL, Strathmann TJ. Visible-light-mediated TiO_2 photocatalysis of fluoroquinolone antibacterial agents. *Environ. Sci. Technol*. 2007;41:4720-4727.
48. Guo H, Jiang N, Wang HJ, et al. Enhanced catalytic performance of graphene-TiO_2 nanocomposites for synergetic degradation of fluoroquinolone antibiotic in pulsed discharge plasma, *Appl. Catal. B: Environ*. 2019;248:552-566.
49. Vaizoğullar Aİ. TiO_2/ZnO supported on sepiolite: preparation, structural characterization, and photocatalytic degradation of flumequine antibiotic in aqueous solution. *Chem. Eng. Commun*. 2017;204:689-697.